A20 restriction of nitric oxide production restores macrophage bioenergetic balance

Mei-po Chan[1], Rommel Advincula[1], Philip Achacoso[1], Elizabeth A. Grossman[2], Daniel K. Nomura[2], Barbara A. Malynn[1], and Averil Ma[1*]

[1]Department of Medicine, University of California, San Francisco, San Francisco, CA. 94143

[2]Departments of Chemistry, Molecular and Cell Biology, and Nutritional Sciences and Toxicology, University of California, Berkeley, Berkeley, CA 94720

*Correspondence to: Averil Ma, MD, 513 Parnassus Ave, S-1032C, University of California, San Francisco, San Francisco, CA. 94143. Email: Averil.ma@ucsf.edu

Short running title: A20 preserves mitochondrial function

Abstract

Macrophages play critical roles in regulating host responses to microbial pathogens and other forms of tissue stress and can acquire pro-inflammatory or tissue reparative phenotypes. A20, or TNFAIP3, is a potent regulator of innate immune cell functions and is extensively linked to human inflammatory and autoimmune diseases. We now find that A20 is a powerful regulator of both glycolytic and mitochondrial respiration in macrophages. Differentiated macrophages that are acutely rendered A20 deficient exhibit increased glycolytic activity and markedly decreased mitochondrial respiration after LPS stimulation. These cells are unable to repolarize from an M1-like to M2-like phenotype. Compromised mitochondrial oxygen consumption in A20 deficient macrophages is caused by increased nitric oxide production. Inhibition or genetic ablation of inducible nitric oxide synthase (iNOS) restores mitochondrial oxidative phosphorylation and lactate production in these cells. These metabolic perturbations occur independently of exaggerated cytokine production and despite robust production of IL-10. Therefore, A20 prevents Warburg-like aerobic glycolysis and restores macrophage homeostasis.

57

58 **Introduction**

59 Activation of immune cells is associated with a rapid burst in glycolytic activity along with
60 mitochondrial remodeling (Buck et al., 2016). Several days post-activation, T cells return to
61 more basal states associated with lower glycolysis and persistently increased mitochondrial
62 respiration (Makowski et al., 2020). This latter transition may be important for maintaining an
63 epigenetic state that retains physiological memory of past cellular exposures. It may also
64 facilitate feedback mechanisms that control the duration and longitudinal character of immune
65 responses.

66

67 Though less studied than T cells, macrophages appear to undergo similar metabolic changes
68 during activation with ligands such as LPS (O'Neill and Pearce, 2016; Galván-Peña and O'Neill,
69 2014). Initial LPS stimulation of these cells triggers a glycolytic surge that provides energy for
70 cytokine transcription, translation, and secretion. Subsequent subsiding of glycolysis with a
71 relative shift back to mitochondrial oxidative phosphorylation coincides with transitions to
72 relative LPS tolerance or to cells that express anti-inflammatory molecules associated with
73 wound repair and tissue restoration, e.g., M2 macrophages. Importantly, while selected
74 metabolic enzymes have been implicated in these processes (Mills et al., 2016), the cell
75 biological mechanisms that couple immune cell activation with metabolic shifts are
76 incompletely understood.

77

78 The ubiquitin editing protein A20, also known as TNF-α-induced protein 3 (TNFAIP3), is a
79 susceptibility gene for multiple diseases including rheumatoid arthritis, Crohn's disease,
80 systemic lupus erythematosus, psoriasis, multiple sclerosis, scleroderma, and asthma (Ma and
81 Malynn, 2012). In addition, patients with mono-allelic loss-of-function mutations of A20
82 develop mucosal and skin ulcers resembling Behçet's disease as well as a growing number of
83 other autoinflammatory and autoimmune disorders (Zhou et al., 2016; Ohnishi et al., 2017;
84 Takagi et al., 2017; Aeschlimann et al., 2018). In parallel, A20 deficiency or mutations in mice
85 leads to the development of spontaneous inflammation and autoimmune phenotypes (Boone
86 et al., 2004; Lee et al., 2000; Tavares et al., 2010; Razani et al., 2020). Mice lacking A20 in
87 selected innate immune cell types exhibit phenotypes that highlight the importance of A20
88 functions in macrophages, dendritic cells, and innate lymphoid cells (Hammer et al., 2011; Kool
89 et al., 2011; Matmati et al., 2011; Schneider et al., 2018). A20 also regulates myelopoiesis, and
90 perturbed myeloid differentiation may contribute to altered functions of mature cells (Muto et
91 al., 2020). We have now explored the role of A20 in regulating metabolic transitions of
92 macrophages, using a tamoxifen inducible system that allows myeloid cells to undergo normal
93 hematopoiesis prior to A20 deletion. We find that A20 is a potent regulator of both glycolytic
94 and mitochondrial activity in activated macrophages.
95
96 **Results and Discussion**
97 Induced deletion of A20 in macrophages promotes aerobic glycolysis
98 To understand how A20 regulates macrophage functions independently from developmental
99 events, we interbred $A20^{Flox/Flox}$ mice with mice bearing the ROSA/ER-Cre gene (Tavares et al.,

100 2010). We generated bone marrow derived macrophages (BMDMs) from the resulting
101 A20$^{Flox/Flox}$ ROSA/ER-Cre+, A20$^{Flox/+}$ ROSA/ER-Cre-, and A20$^{Flox/Flox}$ ROSA/ER-Cre- mice, and
102 established conditions for deleting A20 from A20$^{Flox/Flox}$ ROSA/ER-Cre+ bone marrow cells *in*
103 *vitro*. We call these cells A20^{tiKO} BMDMs. While Cre negative BMDMs induced expression of A20
104 protein within one hour after LPS stimulation, which gradually returned to basal levels over 16
105 hours, stimulation of A20^{tiKO} BMDMs expressed no detectable protein (**Fig. 1A**). LPS stimulation
106 of A20^{tiKO} cells caused increased production of pro-inflammatory cytokines such as TNF and IL-6
107 when compared with control BMDMs, consistent with prior findings with A20$^{-/-}$ BMDMs (**Fig.**
108 **1B**) (Boone et al., 2004; Turer et al., 2008). As macrophages develop tolerance to LPS and are
109 thought to restore homeostatic functions after 16-48 hours (Seeley and Ghosh, 2017; Kotwal
110 and Chien, 2017), we studied macrophages 24 hours after LPS stimulation. Remarkably, LPS
111 stimulation of A20^{tiKO} BMDMs led to visibly changed media when compared to control cells (**Fig.**
112 **1C**). As culture medium acidification is most commonly caused by a change in lactate
113 production, lactate levels in the culture supernatants were measured. A20^{tiKO} BMDMs produced
114 markedly more lactate than control cells at 18 and 24 hours after LPS stimulation (**Fig. 1D**). This
115 exaggerated lactate production was not observed after stimulation with other TLR ligands (**Fig.**
116 **1E**). FACS analyses revealed that cell survival was similar in A20^{tiKO} and WT BMDMs at 24 hours
117 post LPS stimulation (**Fig. 1F**). As lactate is an end product of glycolysis, we measured glycolytic
118 activity of these cells via Seahorse extracellular proton flux assay. Prior to LPS stimulation, both
119 A20^{WT} and A20^{tiKO} BMDMs exhibited a similarly modest extracellular acidification rate (ECAR)
120 (**Fig. 1G**). Consistent with prior studies (Galván-Peña and O'Neill, 2014), LPS caused increased
121 glycolysis in normal macrophages (**Fig. 1G**). Importantly, after LPS stimulation, the ECAR of

122 A20^{tiKO} cells was markedly higher than in LPS stimulated WT cells (**Fig. 1G**). After
123 rotenone/antimycin A mediated inhibition of mitochondrial respiration, both A20^{tiKO} and WT
124 cells enhanced proton efflux, with A20^{tiKO} cells showing greater glycolytic capacity (**Fig. 1G**). The
125 differential ECAR between maximal glycolytic capacity and basal rate was slightly greater in WT
126 cells, suggesting diminished glycolytic reserve in A20^{tiKO} cells (**Fig. 1G**).
127
128 Figure 1: Inducible deletion of A20 from BMDMs leads to enhanced expression of glycolytic enzymes and glycolytic
129 activity after LPS stimulation. **(A)** Immunoblot of A20 expression in A20$^{Flox/Flox}$ Rosa/ER-Cre ("ER-Cre +" or A20^{tiKO})
130 and A20$^{Flox/Flox}$ ("ER-Cre –") BMDMs after 4-OH-T mediated deletion of A20 followed by LPS stimulation for the
131 indicated number of hours. Data are representative of three independent experiments. **(B)** ELISA of TNF and IL-6
132 secretion from A20^{tiKO} (red columns) and WT (black columns) BMDMs after LPS. Mean values ± SD are shown. ***
133 indicates p<0.001 by Student's T test. Data are representative of three independent experiments. **(C)** Gross images
134 of culture media from A20^{tiKO} and WT BMDMs with or without LPS stimulation. Data are representative of at least
135 three experiments. **(D)** Lactate secretion from BMDMs of indicated genotypes displayed as fold induction of LPS
136 stimulated cells at indicated time points after LPS relative to unstimulated cells. Pooled results from six
137 independent experiments are shown. Mean values ± SD are shown. ** indicates p<0.01 and *** indicates p<0.001
138 by one way ANOVA. **(E)** Lactate secretion from A20^{tiKO} (red columns) and WT (black columns) BMDMs after
139 stimulation with indicated TLR ligands. Mean values ± SD are shown. ** indicates p<0.01 by Student's T test. Data
140 are representative of two independent experiments. **(F)** Flow cytometric quantification of BMDM cell viability via
141 live-dead staining. Data are representative of two independent experiments. Mean values ± SD are shown. **(G)**
142 Extracellular acidification rate (ECAR) of A20^{tiKO} and WT BMDMs with and without LPS stimulation analyzed by
143 Seahorse proton flux assay. Rotenone/antimycin A and 2-deoxyglucose (2-DG) added at indicated times. Mean
144 values ± SD are shown. Data are representative of three independent experiments. **(H)** Real-time quantitative PCR
145 analyses of *glut1, hk2, ldha, gpi1, pkm2* and *hif1a* mRNA expression relative to *actin* mRNA in indicated genotypes

146 of cells at indicated times after LPS stimulation. Mean values ± SD are shown. Data are representative of two
147 independent experiments. All TLR stimulations were conducted for 24 hours unless otherwise stated.
148
149 The glycolytic surge in activated lymphocytes is supported by multiple molecular adaptations.
150 Glut1 is a glucose transporter which is transcriptionally induced in $CD4^+$ T cells, and is essential
151 for their activation and differentiation into effector cells (Macintyre et al., 2014). Hexokinase2
152 phosphorylates intracellular glucose, preventing its transport out of the cell, and represents the
153 first step of glycolysis. Lactate dehydrogenase (LDH) converts pyruvate to lactate and
154 regenerates nicotinamide adenine dinucleotide (NAD) to support glycolysis. Glucose 6
155 phosphate isomerase (GPI) converts glucose-6-phosphate to fructose-6-phosphate and
156 represents the second step of glycolysis. Pyruvate kinase M2 (PKM2) converts
157 phosphoenolpyruvate to pyruvate. HIF1α is a transcription factor that drives expression of
158 several glycolytic enzymes. After LPS stimulation, expression of mRNAs for all these molecules
159 was markedly increased in A20 deficient macrophages when compared to control cells (**Fig. 1H**).
160 Hence, A20 restrains multiple facets of glycolysis that collaborate to limit the glycolytic surge
161 accompanying LPS stimulation. This increased glycolytic activity may support enhanced
162 production and secretion of cytokines by A20 deficient macrophages.
163
164 <u>Induced deletion of A20 in macrophages suppresses mitochondrial respiration and prevents M2</u>
165 <u>repolarization after LPS</u>
166 After LPS stimulation, macrophages can assume tissue reparative functions, reduction of
167 glycolysis, and a return to predominantly mitochondrial oxidative phosphorylation for ATP

168 production. We thus assayed mitochondrial respiration by measuring the oxygen consumption
169 rate (OCR) of A20^{tiKO} and control BMDMs via Seahorse assays. Consistent with prior work, the
170 OCR of WT BMDMs increased after LPS stimulation (**Fig. 2A**). By contrast, A20^{tiKO} BMDMs, which
171 contained mildly elevated levels of OCR when compared to unstimulated WT cells, exhibited
172 markedly decreased OCR after LPS stimulation (**Fig. 2A**, see basal OCR). Oligomycin inhibits ATP
173 synthase and the OCR in oligomycin treated cells reflects the amount of ATP generated by the
174 mitochondrial electron transport chain. A20^{tiKO} BMDMs exhibited negligible decrements of OCR
175 after oligomycin (**Fig. 2A**, see ATP production). FCCP uncouples the proton gradient generated
176 by the electron transport chain, unveiling the maximal oxygen consumption potential of
177 mitochondria in normal cells. While WT cells and unstimulated A20^{tiKO} BMDMs increased their
178 OCR to maximal levels, LPS stimulated A20^{tiKO} BMDMs completely failed to increase their OCR in
179 response to FCCP (**Fig. 2A**, see maximal). Therefore, LPS stimulation cripples the ability of
180 mitochondrial electron transport complexes in A20^{tiKO} BMDMs to consume oxygen even when
181 these complexes are uncoupled from their electron transport functions. The difference
182 between FCCP induced maximal OCR and basal OCR, termed the spare respiratory capacity
183 (SRC), reflects the cell's ability to marshal reserves for energy production and is an indicator of
184 cellular fitness (**Fig. 2A**, see SRC). In this regard, A20^{tiKO} BMDMs displayed negligible SRC. Finally,
185 inhibition of complexes I and III with rotenone and antimycin A blocks mitochondrial respiration
186 and unveils oxygen consumption from non-mitochondrial sources. These treatments revealed
187 modestly increased OCR in A20^{tiKO} BMDMs, consistent with the increased glycolysis observed in
188 these cells. These respiratory defects in A20^{tiKO} BMDMs were triggered by LPS stimulation but
189 not by other TLR ligands such as Pam_3CSK_4 and polyI:C (**Figs. 2B, 2C**). Hence, while A20^{tiKO}

190 BMDMs conduct increased glycolysis after LPS stimulation, these cells perform markedly less
191 mitochondrial respiration, thereby exhibiting a profound bioenergetic bias toward aerobic
192 glycolysis. This dramatic metabolic shift from oxidative phosphorylation to aerobic glycolysis in
193 A20 deficient macrophages constitutes a potent version of the Warburg effect initially
194 described in cancer cells. Importantly, as A20 is a tumor suppressor (Schmitz et al., 2009; Kato
195 et al., 2009; Compagno et al., 2009), the loss of this protein could drive aerobic glycolysis in
196 some cancer cells as well.
197
198 Figure 2: LPS activation cripples mitochondrial respiration and prevents M2 repolarization in $A20^{tiKO}$ BMDMs. **(A)**
199 Oxygen consumption rate (OCR) measured by Seahorse flux assay of LPS stimulated A20 deficient (red circles) and
200 WT (black circles) BMDMs. Open circles represent unstimulated cells; Closed circles represent LPS stimulated cells.
201 Mitochondrial stress tests with oligomycin (Oligo), FCCP, and rotenone/antimycin A injected at indicated times
202 (arrows). Calculated levels of basal and maximal mitochondrial respiration, spare respiratory capacity (SRC) and
203 ATP production shown at right. Mean values ± SD are shown. *** indicates $p<0.001$ by unpaired two-tailed T test.
204 Data are representative of at least five independent experiments. **(B and C)** Mitochondrial stress tests of $A20^{WT}$
205 and $A20^{tiKO}$ BMDMs after stimulation with Pam_3CSK_4 (**B**) or polyI:C (**C**). Mean values ± SD are shown. Data are
206 representative of three independent experiments. **(D)** Schematic representation of experimental design of M2
207 repolarization assay. On day 7 of BMDM differentiation, cells were treated with LPS for 24 hours, washed and
208 stimulated with IL-4 or medium for another 24 hours. Flow cytometric measurement of M2 surface markers were
209 assayed on day 9. **(E)** Representative flow cytometric analyses of CD301 and CD206 cell surface expression (M2
210 markers) on $A20^{tiKO}$ and WT BMDMs after IL-4 mediated repolarization as described in (D). Mean values ± SD are
211 shown. Data are representative of two independent experiments. **(F)** Oil red O staining of indicated genotypes of
212 BMDMs after stimulation with LPS. Note lipid droplets inside $A20^{tiKO}$ BMDMs. Scale bars represent 2 µm. Data are
213 representative of three independent experiments.
214

215 The major source of ATP in M2 macrophages derives from oxidative phosphorylation by
216 mitochondria (Jha et al., 2015; Vats et al., 2006). Hence, A20's preservation of macrophage
217 mitochondrial function might support M2 repolarization after LPS stimulation. We tested the
218 ability of LPS stimulated A20^{tiKO} BMDMs to repolarize to an M2 phenotype after IL-4
219 stimulation. We stimulated A20^{tiKO} and A20^{WT} BMDMs with LPS for 24 hours, treated these cells
220 with IL-4 for another 24 hours, and finally analyzed the expression of M2 markers by FACS (**Fig.**
221 **2D**). A20^{tiKO} BMDMs were largely unable to express the M2 markers CD301 and CD206 after
222 repolarization with IL-4 (**Fig. 2E**). Instead, A20^{tiKO} BMDMs were strongly stained with Oil Red O,
223 indicating enhanced lipid droplet formation and accumulation after LPS stimulation (**Fig. 2F**), a
224 hallmark of inflammatory M1 macrophages (Rosas-Ballina et al., 2020; Wen et al., 2011). Such
225 lipid droplets have been described as sites of eicosanoid synthesis, enzyme localization and
226 cytokine storage in inflammatory leukocytes (Bozza and Viola, 2010; Jarc and Petan, 2020).
227 Hence, A20 is required for the ability of activated macrophages to express type 2 markers and
228 potentially evolve into cells supporting tissue repair. The persistence of M1 associated proteins
229 likely contributes to the ability of these cells to drive inflammatory diseases.
230
231 <u>Mitochondria in A20 deficient macrophages exhibit defective membrane potential and</u>
232 <u>compromised turnover</u>
233 Healthy mitochondria generate an electrochemical proton gradient that fuels the electron
234 transport chain and ATP generation. To better understand how A20 maintains mitochondrial
235 respiration in LPS stimulated macrophages, we first measured the mitochondrial membrane
236 potential in A20^{WT} and A20^{tiKO} cells. Consistent with our Seahorse assays (**Fig. 2A**), A20^{tiKO}

237 BMDMs exhibited decreased transmembrane potential after LPS stimulation (**Fig. 3A**). This
238 decreased membrane potential was not associated with reduced mitochondrial mass, as the
239 ratio of mitochondrial DNA to nuclear DNA was preserved in A20^{tiKO} BMDMs (**Fig. 3B**).
240 Immunoblotting analyses of the mitochondrial protein Tomm20 revealed normal amounts of
241 this protein in both unstimulated and LPS stimulated A20^{tiKO} BMDMs, reinforcing the notion
242 that mitochondrial mass is preserved in these cells (**Fig. 3C**). Taken together, these results
243 indicate that mitochondria are structurally intact, but functionally compromised in LPS
244 stimulated A20^{tiKO} BMDMs.
245
246 Figure 3: Mitochondria in A20^{tiKO} BMDMs exhibit lower membrane potential and decreased turnover. **(A)** FACS
247 mediated measurement of mitochondrial transmembrane potential using tetramethylrhodamine methyl ester
248 (TMRM) labeling. Representative histograms of fluorescent TMRM expression in BMDMs of the indicated
249 genotypes shown at left. Percentage change in TMRM staining calculated at right from three independent
250 experiments. Mean values ± SD are shown. ** indicates $p< 0.01$ by unpaired T test. **(B)** Real time qPCR analyses
251 of mitochondrial and nuclear DNA from the indicated BMDMs. Mean values ± SD are shown. *** indicates
252 $p<0.001$. Data are representative of two independent experiments. **(C)** Immunoblot analysis of mitochondrial
253 Tomm20 protein expression in indicated BMDMs. GAPDH expression shown below as loading control. Data are
254 representative of three independent experiments. **(D)** FACS analyses of mitochondrial turnover using differential
255 labeling. BMDMs were first labeled with MitoTracker Green FM (MTG), then stimulated with LPS, and
256 subsequently labeled with MitoTracker Red (MTR) prior to FACS analysis. In this format, MTG represent pre-
257 existing (old) mitochondria; MTR represent all mitochondria present after LPS stimulation. Note that A20tiKO cells
258 retain a higher proportion of MTG positive (old) mitochondria than WT cells, particularly after LPS stimulation
259 (52.7% vs. 27.7%). Data are representative of three independent experiments. **(E)** Mass spectrometric
260 quantification of indicated tricarboxylic acid (TCA) cycle intermediates in A20^{tiKO} (red) and WT (black) BMDMs after
261 LPS stimulation. Counts reflect average of five replicates. **(F)** Fluorometric assay of citrate synthase (CS) activity of

262 indicated cells after LPS stimulation was measured. **(G)** FACS analyses of mitochondrial superoxide production in
263 A20^{tiKO} and WT BMDMs using using mitoSOX dye (mSOX). Data are representative of three independent
264 experiments.
265
266 During metabolically demanding cellular activation events, damaged mitochondria undergo
267 conformational changes and turnover to preserve the quantity and quality of these organelles
268 (Gkikas et al., 2018). We thus assessed mitochondrial turnover in A20^{WT} and A20^{tiKO} BMDMs.
269 We utilized differential labeling of mitochondria using MitoTracker Green (MTG) and
270 MitoTracker Red (MTR) before and after LPS stimulation, to quantitate pre-existing and newly
271 generated mitochondria. A20^{tiKO} BMDMs contained a larger fraction of older, pre-existing
272 (MTG+) mitochondria than WT BMDMs without LPS, suggesting that basal mitochondrial
273 turnover is compromised in A20^{tiKO} cells (**Fig. 3D**). This difference became much more
274 pronounced after LPS stimulation, indicating that A20 may be particularly important for
275 replacing senescent mitochondrial in activated macrophages (**Fig. 3D**). A20 dependent
276 mitochondrial replacement thus appears to collaborate with A20's ability to preserve
277 mitochondrial OCR in a coordinated effort to preserve cellular energetic homeostasis.
278
279 To further investigate the defective mitochondrial respiration in A20 deficient macrophages, we
280 performed targeted metabolomic studies on LPS stimulated cells. These assays revealed that
281 A20^{tiKO} BMDMs contain similar levels of the tricarboxylic acid (TCA) cycle intermediates,
282 succinate, citrate and α-ketoglutarate (α-KG) as control cells, suggesting that TCA cycling
283 proceeds at sufficient rates in these cells to generate electron donors and substrates to the
284 mitochondrial electron transport chain (**Fig. 3E**). We also directly assayed the activity of citrate

285 synthase, the enzyme catalyzing the condensation between oxaloacetate and acetyl Co-A to
286 generate citrate. This enzyme is considered the first step of the TCA cycle. These tests showed
287 that citrate synthase activity was preserved in A20^{tiKO} BMDMs throughout 24 hours of LPS
288 stimulation (**Fig 3F**). As the levels of citrate and succinate were comparable in WT and A20
289 deficient macrophages, previously described inhibition of these TCA cycle steps do not appear
290 to depend upon A20 (Tannahill et al., 2013; Liu et al., 2017; Jha et al., 2015). Finally, as
291 increased release of mitochondrial superoxide can cause dysfunctional mitochondria with
292 augmented electron leaks, we measured oxidation of the superoxide indicator, MitoSOX (**Fig.**
293 **3G**). During the 24 hours of LPS stimulation, MitoSOX levels remained similar between A20^{WT}
294 and A20^{tiKO} cells, implying that impaired mitochondrial respiration in A20^{tiKO} cells was not
295 caused by excessive induction of mitochondrial superoxide. Taken together, these data suggest
296 that acute A20 deficiency in macrophages causes defective mitochondrial respiration despite
297 the availability of comparable TCA substrates and structurally intact mitochondria.
298
299 <u>A20 deficient macrophages accumulate increased reactive oxygen and nitrogen species, and</u>
300 <u>exaggerated inducible nitric oxide synthase (iNOS) expression compromises mitochondrial</u>
301 <u>respiration</u>
302 Elevated cellular reactive oxygen species (ROS) and reactive nitrogen species (RNS) can
303 compromise mitochondrial function by inhibiting electron transport chain enzymes (Kaludercic
304 and Giorgio, 2016; Kowalska et al., 2020). Our metabolomic analyses revealed markedly
305 decreased glutathione (GSH) levels in LPS stimulated A20^{tiKO} BMDMs (**Fig. 4A**). In addition,
306 glycine, an essential and rate-limiting precursor of GSH, was also significantly lower in these

307 BMDMs (**Fig. 4A**). As GSH is a major cellular antioxidant that reacts with and scavenges
308 potentially deleterious ROS and RNS, we hypothesized that A20 deficient macrophages might
309 accumulate excessive amounts of these reactive species. We measured cellular ROS/RNS levels
310 using the fluorescent indicator dichlorodihydrofluorescein diacetate (DCFDA), and found that
311 A20^{tiKO} BMDMs exhibited significantly higher levels of DCFDA staining after LPS stimulation (**Fig.**
312 **4B**). Among RNS, nitric oxide (NO) and its metabolite peroxynitrite inhibit electron transport
313 chain enzymes by binding to O_2 binding sites on these proteins (Stewart and Heales, 2003). We
314 assayed NO levels and found that A20^{tiKO} BMDMs produced markedly more NO than control
315 cells after LPS (**Fig. 4C**). This exaggerated NO production was not observed after stimulation
316 with other TLR ligands (**Fig. 4C**). We next tested whether abrogating production of these species
317 might restore mitochondrial defects. While allopurinol, a xanthine oxidase inhibitor, did not
318 rescue OCR defects in LPS stimulated A20^{tiKO} BMDMs (**Fig. 4D**), the iNOS inhibitor 1400w
319 effectively restored mitochondrial respiration (**Fig. 4E**) and M2 repolarization (**Suppl. Fig. 1**).
320
321 Figure 4: A20^{tiKO} BMDMs produce exaggerated amounts of nitric oxide (NO), and impaired mitochondrial
322 respiration is rescued by inhibition of nitric oxide synthase (iNOS). **(A)** Mass spectrometric quantification of
323 reduced and oxidized forms of glutathione (GSH) (left graph) and glycine (right graph) in A20^{tiKO} (red) and WT
324 (black) BMDMs after LPS stimulation. * indicates $p<0.05$, ** indicates $p<0.01$, *** indicates $p<0.001$. Data are
325 representative of 5 independent samples. **(B)** Flow cytometric analyses of cytosolic ROS/RNS species in LPS treated
326 BMDMs of the indicated genotypes using dichlorodihydrofluorescein diacetate (DCFDA) dye. Y-axis represents
327 geometric mean fluorescence intensity (gMFI) of each sample relative to untreated cells at the indicated
328 timepoints after LPS stimulation. * indicates $p<0.05$, ** indicates $p<0.01$. Mean values ± SD are shown. Pooled
329 results from five independent experiments are shown. **(C)** Calorimetric determination of nitric oxide (NO)
330 production from A20^{tiKO} (red) and WT (black) BMDMs after stimulation with the indicated TLR ligands. Mean values

331 ± SD are shown. *** indicates p<0.001. Data are representative of three independent experiments. **(D)** Seahorse
332 mitochondrial stress test of A20^{tiKO} (red) and WT (black) BMDMs with or without xanthine oxidase inhibitor
333 allopurinol (allo). Mean values ± SD are shown. Data are representative of three independent experiments. **(E)**
334 Seahorse mitochondrial stress test of A20^{tiKO} (red) and WT (black) BMDMs with or without iNOS inhibitor 1400w.
335 Basal and maximal respiratory rates, spare respiratory capacity (SRC), and ATP production are shown at right.
336 Mean values ± SD are shown. *** indicates p<0.001. Data are representative of three independent experiments. In
337 all panels, * indicates p<0.05, ** indicates p<0.01, *** indicates p<0.001 using unpaired two-tailed t test.
338

339 NO is produced by several nitric oxide synthase enzymes that are expressed in multiple cell
340 types. To understand why A20^{tiKO} BMDMs secreted excessive amount of NO after LPS
341 stimulation, we measured the expression of iNOS (*nos2*), the inducible isoform of NOS that is
342 robustly expressed in macrophages and generates NO in a Ca^{++} independent fashion
343 (Förstermann and Sessa, 2012). While resting BMDMs express negligible levels of iNOS mRNA
344 and protein, these species were both expressed at markedly higher levels in A20^{tiKO} BMDMs
345 than control cells after LPS stimulation (**Figs. 5A, B**). To define the contribution of iNOS to
346 mitochondrial dysfunction in A20^{tiKO} BMDMs, we interbred A20$^{Flox/Flox}$ ROSA/ER-Cre mice with
347 iNOS$^{-/-}$ mice (Laubach et al., 1995) and tested LPS responses of the compound mutant
348 macrophages derived from these mice. Immunoblot analyses of A20 and iNOS expression
349 confirmed elimination of these proteins in the appropriate genotypes (**Suppl. Fig. 2**).
350 Stimulation of A20^{tiKO} iNOS$^{-/-}$ BMDMs with LPS resulted in normalization of cellular ROS/RNS
351 levels when compared with A20^{tiKO} BMDMs (**Fig. 5C**). Hence, iNOS is predominantly responsible
352 for the exaggerated ROS/RNS species generated in LPS stimulated A20^{tiKO} BMDMs. Similar
353 results were obtained with the iNOS inhibitor 1400w (**Suppl. Fig. 3**). Remarkably, extracellular

354 flux assays revealed that ablation of iNOS completely restored mitochondrial respiration in
355 A20^{tiKO} BMDMs (**Fig. 5D).** These A20^{tiKO} iNOS$^{-/-}$ BMDMs also exhibited normal levels of ATP
356 production and spare respiratory capacity (**Fig. 5D**). In addition to restoring deficient
357 mitochondrial respiration, abrogation of iNOS expression also normalized the exaggerated
358 lactate production observed in A20^{tiKO} BMDMs (**Fig. 5E**). Therefore, iNOS expression is a
359 dominant mechanism regulating the balance between glycolytic and mitochondrial respiration.
360

361 Figure 5: Expression of iNOS is greatly induced in A20^{tiKO} BMDMs, and genetic ablation of *nos2* restores
362 mitochondrial bioenergetic balance. **(A)** Real-time qPCR analyses of *nos2* mRNA expression relative to *actin* mRNA
363 in A20^{tiKO} (red) and A20^{WT} (black) BMDMs at indicated timepoints after LPS stimulation. Mean values ± SD are
364 shown. *** indicates p<0.001 by unpaired T test. Data are representative of three independent experiments. **(B)**
365 Immunoblot analyses of iNOS protein expressions in indicated BMDMs at indicated timepoints after LPS
366 stimulation. GAPDH protein expression shown below as loading control. The iNOS inhibitor 1400w inhibits iNOS
367 activity rather than iNOS expression and is shown as a control. Data are representative of three independent
368 experiments. **(C)** Flow cytometry analysis of ROS/RNS species by DCFDA staining in the indicated genotypes of
369 BMDMs after LPS stimulation. DCFDA staining intensity is plotted relative to unstimulated cells. Note that
370 increased ROS/RNS in LPS stimulated A20^{tiKO} cells (red) is normalized in LPS stimulated A20^{tiKO} iNOS$^{-/-}$ cells (blue).
371 Mean values ± SD are shown. * indicates p<0.05, ** indicates p<0.01. Data are representative of three
372 independent experiments. **(D)** Seahorse mitochondrial stress test of BMDMs from the indicated genotypes of mice.
373 Note that depressed basal and maximal oxygen consumption rates (OCR) in A20^{tiKO} cells (red) is normalized in LPS
374 stimulated A20^{tiKO} iNOS$^{-/-}$ cells (blue). Graphic representation of basal and maximal OCRs, spare respiratory
375 capacity (SRC), and ATP production are shown below. Mean values ± SD are shown. *** indicates p<0.001. Data
376 are representative of four independent experiments. **(E)** Colorimetric measurements of lactate secretion by
377 indicated genotypes of cells. Mean values ± SD are shown. * indicates p< 0.05, ** indicates p<0.01 by unpaired T
378 test. Data are representative of three independent experiments. **(F)** Real-time quantitative PCR analyses of *tnf, il-6*

379 *and ifnb1* mRNA expression relative to *actin* in the respective BMDMs after LPS stimulation. Mean values ± SD are
380 shown. Data are representative of three independent experiments. **(G)** ELISA of IL-1β secretion by $A20^{WT}$ and
381 $A20^{tiKO}$ and WT BMDMs after indicated treatments. Mean values ± SD are shown. * indicates $p<0.05$, *** indicates
382 $p<0.001$. Data are representative of two independent experiments. **(H)** ELISA of IL-10 secretion by $A20^{WT}$ and
383 $A20^{tiKO}$ and WT BMDMs after indicated treatments. Mean values ± SD are shown. *** indicates $p<0.001$ by
384 unpaired T test. Data are representative of two independent experiments.
385

386 <u>Resuscitation of mitochondrial respiration in $A20^{tiKO}$ $iNOS^{-/-}$ BMDMs occurs independently from</u>
387 <u>A20 regulated inflammatory cytokines and inflammasome activation</u>

388 A20 deficient macrophage express greater amounts of inflammatory cytokines than control
389 cells in response to LPS stimulation (Boone et al., 2004; Turer et al., 2008). These cytokines
390 could theoretically contribute to mitochondrial dysfunction in $A20^{tiKO}$ BMDMs. We tested
391 cytokine responses in $A20^{tiKO}$ and $A20^{tiKO}$ $iNOS^{-/-}$ BMDMs after LPS stimulation and found that
392 exaggerated production of TNF, IL-6, and IFN-β mRNAs by $A20^{tiKO}$ BMDMs was not abrogated by
393 elimination of iNOS expression in $A20^{tiKO}$ $iNOS^{-/-}$ BMDMs (**Fig. 5F**). Therefore, iNOS deficiency
394 decouples mitochondrial dysfunction in $A20^{tiKO}$ BMDMs from exaggerated secretion of pro-
395 inflammatory cytokines.
396

397 ROS have been described to mediate a second step to activate NLRP3 inflammasomes (Zhou et
398 al., 2011), and $A20^{-/-}$ BMDMs exhibit aberrant spontaneous NLRP3 inflammasome activation,
399 i.e., secretion of mature IL-1β after LPS without ATP stimulation (Walle et al., 2014; Duong et
400 al., 2015). Hence, exaggerated NO produced in $A20^{tiKO}$ BMDMs might drive aberrant NLRP3
401 inflammasome activation by generating ROS that activate these protein complexes. We

402 measured IL-1β secretion by ELISA, and found that A20^{tiKO} BMDMs secreted IL-1β even in the
403 presence of the iNOS inhibitor 1400w that restored mitochondrial respiration (**Fig. 5G**). Hence,
404 A20 regulates mitochondrial respiration via a distinct cell biological pathway from its regulation
405 of inflammasome activation.
406
407 IL-10 deficient macrophages exhibit defects in mitochondrial function after LPS stimulation (Ip
408 et al., 2017). Hence, A20 deficient macrophages might develop mitochondrial dysfunction due
409 to defective IL-10 production. We assayed IL-10 secretion from LPS stimulated A20^{tiKO} and
410 control BMDMs, and found that A20^{tiKO} cells secreted significantly more IL-10 than control cells
411 (**Fig. 5H**). In addition, while mitochondrial defects in IL-10 deficient macrophages do not depend
412 upon NO (Ip et al., 2017), this reactive nitrogen species is critical for compromising
413 mitochondrial respiration in A20 deficient cells. Thus, A20 and IL-10 appear to control
414 mitochondrial function via distinct mechanisms. Nevertheless, the shared metabolic defects of
415 IL-10 deficient and A20 deficient macrophages may underlie overlapping links of these two
416 molecules to early onset inflammatory bowel disease and other inflammatory diseases.
417
418 In summary, our findings reveal a profound role for A20 in restraining aerobic glycolysis and
419 supporting metabolic reprogramming toward oxidative phosphorylation. The metabolic impact
420 of A20 on macrophage homeostasis is mediated by iNOS and NO. A20 deficient macrophages
421 share some mitochondrial defects with IL-10 deficient macrophages, but are distinguished by
422 the secretion of high levels of IL-10 and reliance upon iNOS. As A20 deficient macrophages may
423 contribute to inflammatory processes in an expanding array of human diseases, including

424 haploinsufficient A20 patients, understanding the metabolic defects found in these cells should
425 open novel avenues toward controlling these clinical syndromes. Finally, as A20 is a tumor
426 suppressor in both mice (Shao et al., 2013) and humans (Kato et al., 2009; Compagno et al.,
427 2009), the severe skewing toward aerobic glycolysis in A20 deficient macrophages suggests that
428 loss of A20 may also support tumorigenesis via metabolic mechanisms as well as via regulation
429 of cell survival pathways.
430
431 **Materials and Methods**
432
433 Mice
434 $A20^{Flox}$ mice were generated in our laboratory and described previously (Tavares et al., 2010).
435 Rosa/ER-Cre mice and $iNOS^{-/-}$ mice were purchased from Jackson Laboratories. All animal
436 research was approved by University of California San Francisco (UCSF) Office of Ethics and
437 Compliance.
438
439 Generation of bone marrow derived macrophages and treatments
440 Bone marrow derived macrophages were prepared as previously described (Duong et al., 2015).
441 Deletion of A20 *in vitro* was performed by adding 60nM 4-hydroxytamoxifen (4-OHT) 2 days
442 before harvested. The doses of ligands used were as follows: lipopolysaccharide 100 ng/ml;
443 poly(I:C) HMW 20 μg/ml; Pam_3CSK_4 1 μg/ml; CpG-A 2 μM; CpG-B 250 nM, Gardiquimod 1
444 μg/ml; PolyU (complexed with lipofectamine) 0.5 μg/ml and flagellin (from *S. typhimurium*) 2
445 μg/ml (Invivogen). For pharmacological inhibitors: allopurinol 25 μM and 1400w 100 μM
446 (Sigma). For macrophage repolarization, cells were stimulated with LPS for 24 hours and
447 washed twice before the addition of 200 ng/ml IL-4 for another 24 hours (PeproTech). The

448 resulting cells were analyzed by flow cytometry (BD Fortessa) at the UCSF Parnassus Flow Core,
449 RRID:SCR_01826, and the software FlowJo (BD).
450
451 NO, ROS and lactate assays
452 Culture supernatants from stimulated macrophages were briefly centrifugated to remove any
453 cell debris. Nitric oxide (NO) was measured using a Total Nitric Oxide Assay kit (Invitrogen). To
454 measure intracellular ROS/RNS, macrophages were loaded with 25 μM H_2DCFDA (Sigma) in
455 serum-free DMEM medium and incubated for 30 min at 37 °C. Cells were then collected,
456 washed once with PBS and resuspended in FACS buffer (2.5% FBS, 0.1% sodium azide, 0.02%
457 sodium bicarbonate in PBS) supplemented with 7-AAD at a working concentration of 2.5 μg/ml
458 for the exclusion of dead cells, and analyzed by flow cytometry (BD Fortessa) at the UCSF
459 Parnassus Flow Core, RRID:SCR_01826, and the software FlowJo (BD). Lactate secretion was
460 measured using a colorimetric Lactate Assay kit (BioVision). All assays were performed
461 according to manufacturer's instructions.
462
463 Mitochondrial assays
464 Mitochondrial membrane potential was measured using tetramethylrhodamine methyl ester
465 (TMRM) (Invitrogen) according to manufacturer's instruction. TMRM (20 nM) was added and
466 incubated for 30 minutes in 37°C CO_2 incubator before cell harvest. Mitochondrial turnover was
467 examined by first labeling mitochondria in unstimulated cells with MitoTracker Green FM
468 (MTG) (Invitrogen) for 30 minutes according to manufacturer's instructions. Cells were then
469 washed twice with PBS and stimulated with LPS for 24 hours. MitoTracker Red CM-H_2Xros

470 (MTR) (Invitrogen) was then added to the culture 30 minutes before harvest in 37°C CO_2
471 incubator. Dead cells were excluded with LIVE/DEAD Fixable Near-IR Viability Dye (Invitrogen)
472 according to manufacturer's instructions. Fluorescent signals were analyzed with flow
473 cytometry (BD Fortessa) at the UCSF Parnassus Flow Core, RRID:SCR_01826, and the software
474 FlowJo (BD). Mitochondrial DNA (mDNA) to nuclear DNA (nDNA) ration was determined as
475 described in details by Malik and colleagues (Malik et al., 2016) using Quantifast SYBR Master
476 Mix (Qiagen) and analyzed with quantitative real-time PCR (Quantstudio 6 Flex Real-Time PCR
477 Systems from Thermo). To measure the mitochondrial protein Tomm20, cell palettes were
478 subjected to lysis in 1x RIPA lysis buffer (Alfa Aesar) supplemented with complete EDTA-Free
479 Protease Inhibitor Cocktail (Roche), phosphatase inhibitors (1 mM Na_3VO_4 and 10 mM NaF) and
480 10 mM N-ethylmaleimide (Sigma), and centrifuged for 20 minutes (21,000 x g at 4°C).
481 Mitochondrial citrate synthase activity was quantitated using the Citrate Synthase Activity
482 Assay kit (BioVision) according to the manufacturer's instruction. To measure mitochondrial
483 derived superoxide, the superoxide indicator MitoSOX Red (Invitrogen) was used according to
484 manufacturer's instructions. Mitochondrial TCA cycle metabolites, GSH and glycine were
485 measured via mass spectrometry as previously described (Louie et al, 2016; Kohnz et al, 2016).
486 Quantitative real-time PCR
487 Total RNA was extracted from BMDMs after treatment using the RNeasy Mini kit (Qiagen)
488 according to the manufacturer's instructions with on-column DNase I digestion (Qiagen). cDNA
489 was synthesized using the PrimeScript RT-PCR kit (Takara Bio) according to manufacturer's
490 instructions. Quantitative real-time PCR was performed using TaqMan probes on Quantstudio 6
491 Flex Real-Time PCR Systems from Thermo.

492

493 Seahorse assays

494 BMDMs were seeded 2 hours before stimulation on the 24-well Seahorse cell culture plates

495 (Agilent). Cells were stimulated for 24 hours in 37°C CO_2 incubator, after which glycolytic

496 activity was analyzed using the XF Glycolytic Rate Assay Kit (Agilent). For mitochondrial oxygen

497 consumption, the XF Cell Mito Stress Test Kit was used (Agilent). Both tests were performed

498 according to manufacturer's instructions.

499

500 Oil Red O staining

501 BMDMs were seeded on Lab-Tek II 8-well Chamber Slides (Thermo) and stimulated 2 hours

502 after attachment. Cells were harvested by washing in PBS twice and then fixed in 10% NBF

503 (Sigma) at room temperature for 10 minutes. Fixative was removed and fresh 10% NBF was

504 added and allow fixation for another 3 hours. After fixation, cells were washed with ddH_2O

505 twice and subsequently with 60% isopropanol for 5 minutes at room temperature. The samples

506 were left to dry completely overnight. The next day, samples were stained and incubated with

507 Oil Red O solution (0.21% Oil Red O powder, Sigma, dissolved in isopropanol and filtered, let set

508 at room temperature for 20 minutes before use) for 10 minutes at room temperature.

509 Afterwards the dye was removed and ddH_2O immediately added. Cells were washed 4 times

510 with ddH_2O. The slides were allowed to dry and mounted in ProLong Gold Antifade Mountant

511 (Invitrogen) before acquiring images under the microscope (Zeiss Axioscope).

512

513

514 **Acknowledgments**

515 This work was supported by NIH RO1 grants, the UCSF Nutrition and Obesity Research Center
516 (P30DK098722) and the UCSF Liver Center (P30DK026743) from the National Institute of
517 Diabetes and Digestive and Kidney Diseases. Author contributions: M. Chan, B. Malynn, A. Ma
518 conceptualized the study, designed and interpreted the experiments, and wrote the
519 manuscript. M. Chan performed and analyzed the experiments. E. Grossman and D. Nomura
520 performed and analyzed metabolomic experiments. R. Advincula and P. Achacoso assisted with
521 mouse breeding and experiments. The authors declare no competing financial interests.

522

523 **References**

524

525 Aeschlimann FA, Batu ED, Canna SW, Go E, Gül A, Hoffmann P, et.al. A20 haploinsufficiency
526 (HA20): clinical phenotypes and disease course of patients with a newly recognised NF-
527 kB-mediated autoinflammatory disease. Ann Rheum Dis. 2018;77: 728–735.

528 Boone DL, Turer EE, Lee EG, Ahmad RC, Wheeler MT, Tsui C, et. al. The ubiquitin-modifying
529 enzyme A20 is required for termination of Toll-like receptor responses. Nat Immunol.
530 2004;5:1052–1060.

531 Bozza PT, and Viola JPB. Lipid droplets in inflammation and cancer. Prostaglandins Leukot
532 Essent Fatty Acids. 2010;82:243–250.

533 Buck MD, O'Sullivan D, Klein Geltink RI, Curtis JD, Chang CH, Sanin DE, et al. Mitochondrial
534 dynamics controls T cell fate through metabolic programming. Cell. 2016;166:63–76.

535 Compagno M, Lim WK, Grunn A, Nandula SV, Brahmachary M, Shen Q, et. al. Mutations of
536 multiple genes cause deregulation of NF-kappaB in diffuse large B-cell lymphoma.
537 Nature. 2019;459:717–721.

538 Duong BH, Onizawa M, Oses-Prieto JA, Advincula R, Burlingame A, Malynn BA, et al. A20
539 restricts ubiquitination of pro-interleukin-1β protein complexes and suppresses NLRP3
540 inflammasome activity. Immunity. 2015;42:55–67.

541 Förstermann U, and Sessa WC. Nitric oxide synthases: regulation and function. Eur Heart J.
542 2012;33:829–837.

543 Galván-Peña S, and O'Neill LAJ. Metabolic reprograming in macrophage polarization. Front
544 Immunol. 2014;5:420.

545 Gkikas I, Palikaras K, and Tavernarakis N. The role of mitophagy in innate immunity. Front.
546 Immunol. 2018;9-21.

547 Hammer GE, Turer EE, Taylor KE, Fang CJ, Advincula R, Oshima S, et.al. Expression of A20 by
548 dendritic cells preserves immune homeostasis and prevents colitis and
549 spondyloarthritis. Nat Immunol. 2011;12:1184–1193.

550 Ip WKE, Hoshi N, Shouval DS, Snapper S, and Medzhitov R. Anti-inflammatory effect of IL-10
551 mediated by metabolic reprogramming of macrophages. Science. 2017;356:513–519.

552 Jarc E, and Petan T. A twist of FATe: Lipid droplets and inflammatory lipid mediators. Biochimie.
553 2020;169:69–87.

554 Jha AK, Huang SCC, Sergushichev A, Lampropoulou V, Ivanova Y, Loginicheva E, et. al. Network
555 integration of parallel metabolic and transcriptional data reveals metabolic modules
556 that regulate macrophage polarization. Immunity. 2015;42:419–430.

557 Kaludercic N, and Giorgio V. 2016. The dual function of reactive oxygen/nitrogen species in
558 bioenergetics and cell death: the role of ATP synthase. Oxidative Medicine and Cellular
559 Longevity. 2016:e3869610.

560 Kato M, Sanada M, Kato I, Sato Y, Takita J, Takeuchi K, et. al. Frequent inactivation of A20 in B-
561 cell lymphomas. Nature. 2009;459:712–716.

562 Kohnz RA, Roberts LS, DeTomaso D, Bideyan L, Yan P, Bandyopadhyay, et. al. 2016. Protein
563 sialylation regulates a gene expression signature that promotes breast cancer cell
564 pathogenicity. ACS Chem Biol. 2016;11:2131-2139.

565 Kool M, van Loo G, Waelput W, De Prijck S, Muskens F, Sze M, et. al. The ubiquitin-editing
566 protein A20 prevents dendritic cell activation, recognition of apoptotic cells, and
567 systemic autoimmunity. Immunity. 2010;35:82–96.

568 Kotwal GJ, and Chien S. Macrophage differentiation in normal and accelerated wound healing.
569 Results Probl Cell Differ. 2017;62:353–364.

570 Kowalska M, Piekut T, Prendecki M, Sodel A, Kozubski W, and Dorszewska J. Mitochondrial and
571 nuclear DNA oxidative damage in physiological and pathological aging. DNA and Cell
572 Biology. 2020;39:1410–1420.

573 Laubach VE, Shesely EG, Smithies O, and Sherman PA. Mice lacking inducible nitric oxide
574 synthase are not resistant to lipopolysaccharide-induced death. Proc Natl Acad Sci U S A.
575 1995;92:10688–10692.

576 Lee EG, Boone DL, Chai S, Libby SL, Chien M, Lodolce JP, and Ma A. Failure to Regulate TNF-
577 Induced NF-κB and Cell Death Responses in A20-Deficient Mice. Science.
578 2000;289:2350–2354.

579 Liu PS, Wang H, Li X, Chao T, Teav T, Christen S, et. al. α-ketoglutarate orchestrates macrophage
580 activation through metabolic and epigenetic reprogramming. Nat Immunol.
581 2017;18:985–994.

582 Louie SM, Grossman EA, Crawford LA, Ding L, Camarda R, Huffman TR, et al.. GSTP1 Is a driver
583 of triple-negative breast cancer cell metabolism and pathogenicity. Cell Chem Biol.
584 2016;23:567-578.
585
586 Ma A, and Malynn BA. A20: linking a complex regulator of ubiquitylation to immunity and
587 human disease. Nat Rev Immunol. 2012;12:774–785.

588 Macintyre AN, Gerriets VA, Nichols AG, Michalek RD, Rudolph MC, Deoliveira D, et. al. The
589 glucose transporter Glut1 is selectively essential for CD4 T cell activation and effector
590 function. Cell Metab. 2014;20:61–72.

591 Makowski L, Chaib M, and Rathmell JC. Immunometabolism: From basic mechanisms to
592 translation. Immunol Rev. 2020;295:5–14.

593 Malik AN, Czajka A, and Cunningham P. Accurate quantification of mouse mitochondrial DNA
594 without co-amplification of nuclear mitochondrial insertion sequences. *Mitochondrion*.
595 2016;29:59–64.

596 Matmati M, Jacques P, Maelfait J, Verheugen E, Kool M, Sze M, et. al. A20 (TNFAIP3) deficiency
597 in myeloid cells triggers erosive polyarthritis resembling rheumatoid arthritis. Nat
598 Genet. 2011;43:908–912.

599 Mills EL, Kelly B, Logan A, Costa ASH, Varma M, Bryant CE, et. al. Succinate Dehydrogenase
600 Supports Metabolic Repurposing of Mitochondria to Drive Inflammatory Macrophages.
601 Cell. 2016;167:457-470.e13.

602 Mulvihill MM, and Nomura DK. Metabolomic strategies to map functions of metabolic
603 pathways. Am J Physiol Endocrinol Metab. 2014;307:E237-244.

604 Muto T, Walker CS, Choi K, Hueneman K, Smith MA, Gul Z, et al. Adaptive response to
605 inflammation contributes to sustained myelopoiesis and confers a competitive
606 advantage in myelodysplastic syndrome HSCs. Nat Immunol. 2020;21:535–545.

607 Ohnishi H, Kawamoto N, Seishima M, Ohara O, and Fukao T. A Japanese family case with
608 juvenile onset Behçet's disease caused by TNFAIP3 mutation. Allergology International.
609 2017;66:146–148.

610 O'Neill LAJ and Pearce EJ. Immunometabolism governs dendritic cell and macrophage function.
611 J Exp Med. 2016;213:15–23.

612 Onizawa M, Oshima S, Schulze-Topphoff U, Oses-Prieto JA, Lu T, Tavares R, et al. The ubiquitin-
613 modifying enzyme A20 restricts ubiquitination of the kinase RIPK3 and protects cells
614 from necroptosis. Nat Immunol. 2015;16:618–627.

615 Razani B, Whang MI, Kim FS, Nakamura MC, Sun X, Advincula R, et al. Non-catalytic ubiquitin
616 binding by A20 prevents psoriatic arthritis–like disease and inflammation. Nat Immunol.
617 2020;21:422–433.

618 Rosas-Ballina M, Guan XL, Schmidt A, and Bumann D. Classical activation of macrophages leads
619 to lipid droplet formation without de novo fatty acid synthesis. Front Immunol. 2020;11.

620 Schmitz R, Hansmann M-L, Bohle V, Martin-Subero JI, Hartmann S, Mechtersheimer G, et al.
621 TNFAIP3 (A20) is a tumor suppressor gene in Hodgkin lymphoma and primary
622 mediastinal B cell lymphoma. J Exp Med. 2009;206:981–989.

623 Schneider C, O'Leary CE, von Moltke J, Liang HE, Ang QY, Turnbaugh PJ, et al. A metabolite-
624 triggered tuft cell-ILC2 circuit drives small intestinal remodeling. Cell. 2018;174:271-
625 284.e14.

626 Seeley JJ and Ghosh S. Molecular mechanisms of innate memory and tolerance to LPS. Journal
627 of Leukocyte Biology. 2017;101:107–119.

628 Shao L, Oshima S, Duong B, Advincula R, Barrera J, Malynn BA, and Ma A. A20 restricts wnt
629 signaling in intestinal epithelial cells and suppresses colon carcinogenesis. PLoS One.
630 2013;8:e62223. doi:10.1371/journal.pone.0062223.

631 Stewart VC and Heales SJR. Nitric oxide-induced mitochondrial dysfunction: implications for
632 neurodegeneration. Free Radical Biology and Medicine. 2003;34:287–303.

633 Takagi M, Ogata S, Ueno H, Yoshida K, Yeh T, Hoshino A, et al. Haploinsufficiency of TNFAIP3
634 (A20) by germline mutation is involved in autoimmune lymphoproliferative syndrome.
635 Journal of Allergy and Clinical Immunology. 2017;139:1914–1922.

636 Tannahill G, Curtis A, Adamik J, Palsson-McDermott E, McGettrick A, Goel G, et al. Succinate is a
637 danger signal that induces IL-1β via HIF-1α. Nature. 2013;496:238–242.

638 Tavares RM, Turer EE, Liu CL, Advincula R, Scapini P, Rhee L, et al. The ubiquitin modifying
639 enzyme A20 restricts B cell survival and prevents autoimmunity. Immunity.
640 2010;33:181–191.

641 Turer EE, Tavares RM, Mortier E, Hitotsumatsu O, Advincula R, Lee B, et al. The Journal of
642 Experimental Medicine. 2008;205:451–464.

643 Vats D, Mukundan L, Odegaard JI, Zhang L, Smith KL, Morel CR, et al. Oxidative metabolism and
644 PGC-1β attenuate macrophage-mediated inflammation. Cell Metabolism. 2006;4:13–24.

645 Walle LV, Opdenbosch NV, Jacques P, Fossoul A, Verheugen E, Vogel P, et al Negative regulation
646 of the NLRP3 inflammasome by A20 protects against arthritis. Nature. 2014;512:69–73.

647 Wen H, Gris D, Lei Y, Jha S, Zhang L, Huang MT, et al. Fatty acid–induced NLRP3-ASC
648 inflammasome activation interferes with insulin signaling. Nature Immunology.
649 2013;12:408–415. doi:10.1038/ni.2022.

650 Zhou Q, Wang H, Schwartz DM, Stoffels M, Park YH, Zhang Y, et al. Loss-of-function mutations
651 in TNFAIP3 leading to A20 haploinsufficiency cause an early onset autoinflammatory
652 syndrome. Nat Genet. 2016;48:67–73.

653 Zhou R, Yazdi AS, Menu P, and Tschopp J. A role for mitochondria in NLRP3 inflammasome
654 activation. Nature. 2011;469:221–225.

655

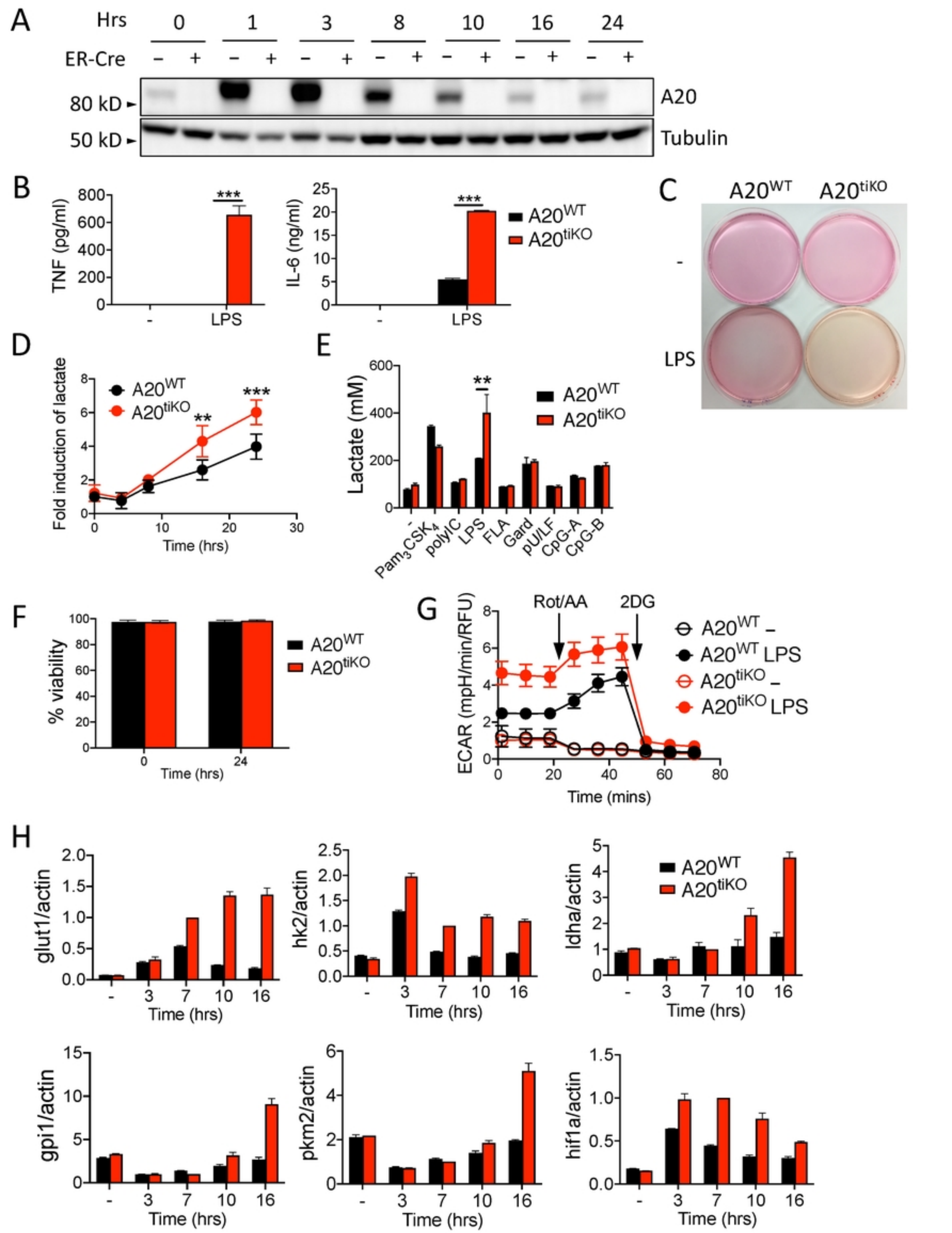
A
Hrs
0
1
3
8
10
16
24
ER-Cre
80 kD
50 kD
A20
Tubulin
B
TNF (pg/ml)
IL-6 (ng/ml)
LPS
A20WT
A20tiKO
C
A20WT
A20tiKO
LPS
D
Fold induction of lactate
Time (hrs)
E
Lactate (mM)
Pam3CSK4
polyIC
FLA
Gard
pU/LF
CpG-A
CpG-B
F
% viability
G
Rot/AA
2DG
ECAR (mpH/min/RFU)
Time (mins)
H
glut1/actin
hk2/actin
ldha/actin
gpi1/actin
pkm2/actin
hif1a/actin

Figure 1

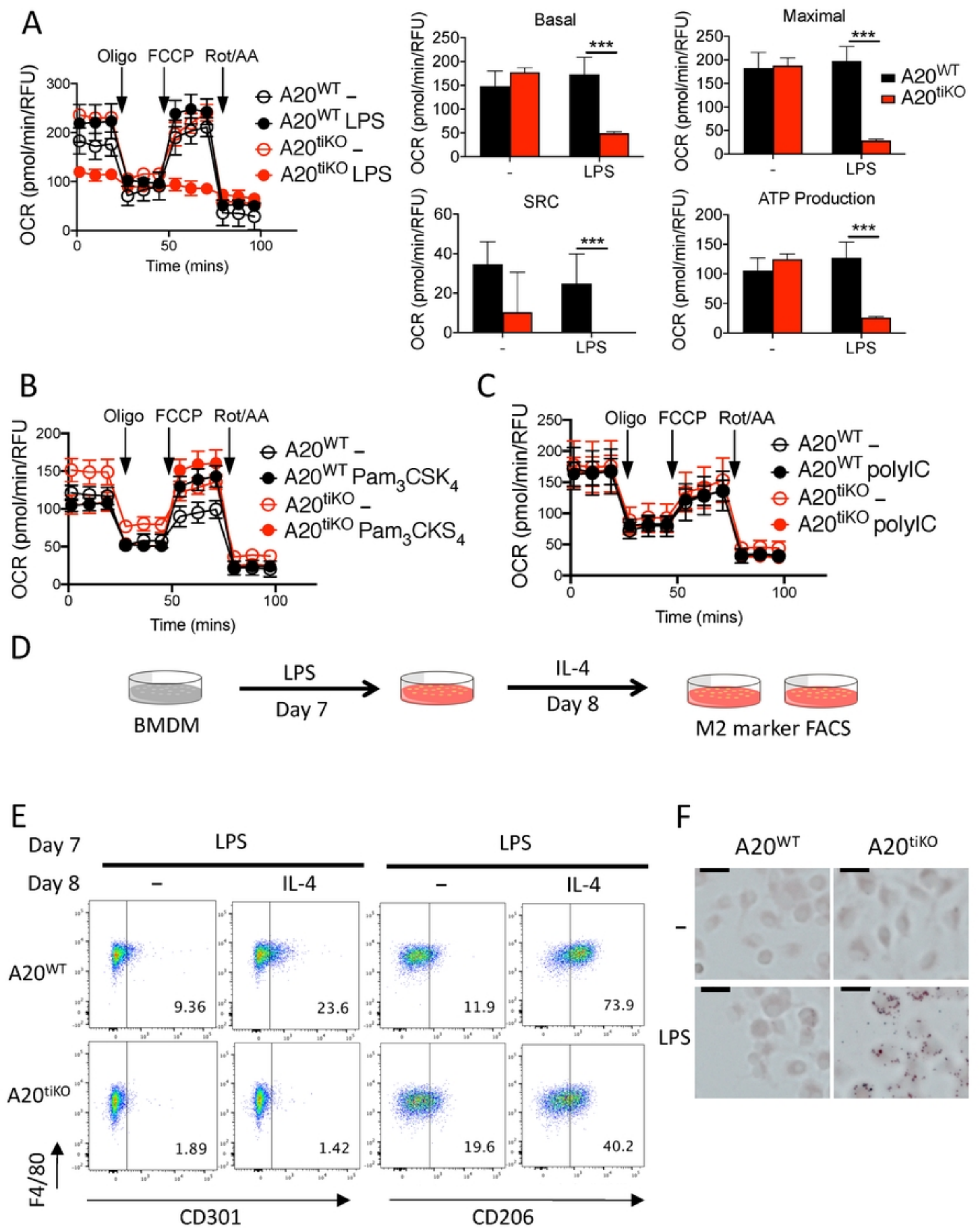
A
Oligo
FCCP
Rot/AA
OCR (pmol/min/RFU)
Time (mins)
A20WT –
A20WT LPS
A20tiKO –
A20tiKO LPS
Basal
Maximal
SRC
ATP Production
***
LPS
A20WT
A20tiKO
B
A20WT Pam3CSK4
A20tiKO Pam3CKS4
C
A20WT polyIC
A20tiKO polyIC
D
LPS
Day 7
IL-4
Day 8
BMDM
M2 marker FACS
E
Day 8
IL-4
A20WT
A20tiKO
9.36
23.6
11.9
73.9
1.89
1.42
19.6
40.2
F4/80
CD301
CD206
F
A20WT
A20tiKO
LPS

Figure 2

Fig 3. : Mitochondria in A20-deficient BMDMs have lower membrane potential and turnover rate, but are mostly intact after LPS stimulation

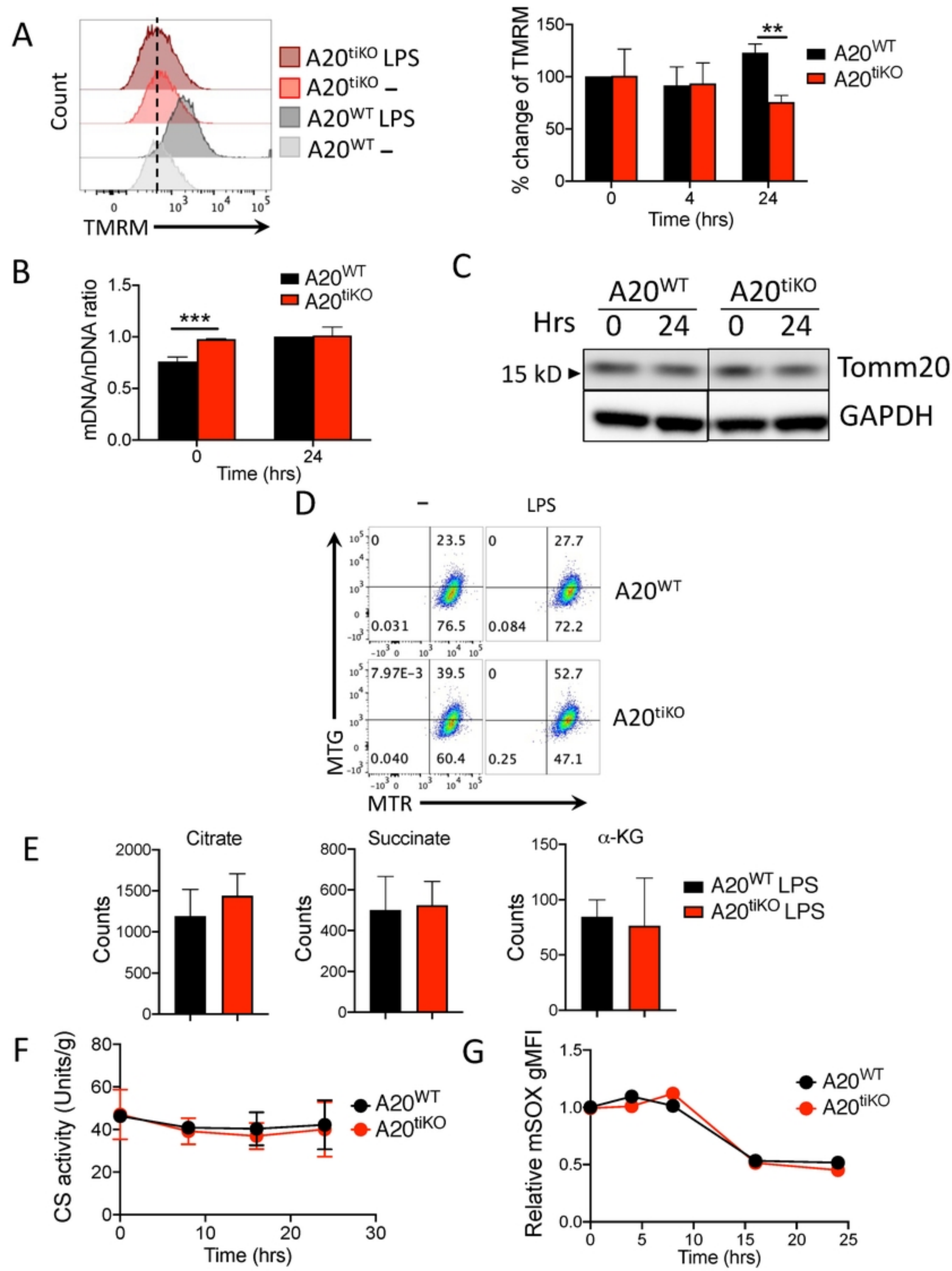

Figure 3

Fig 4.

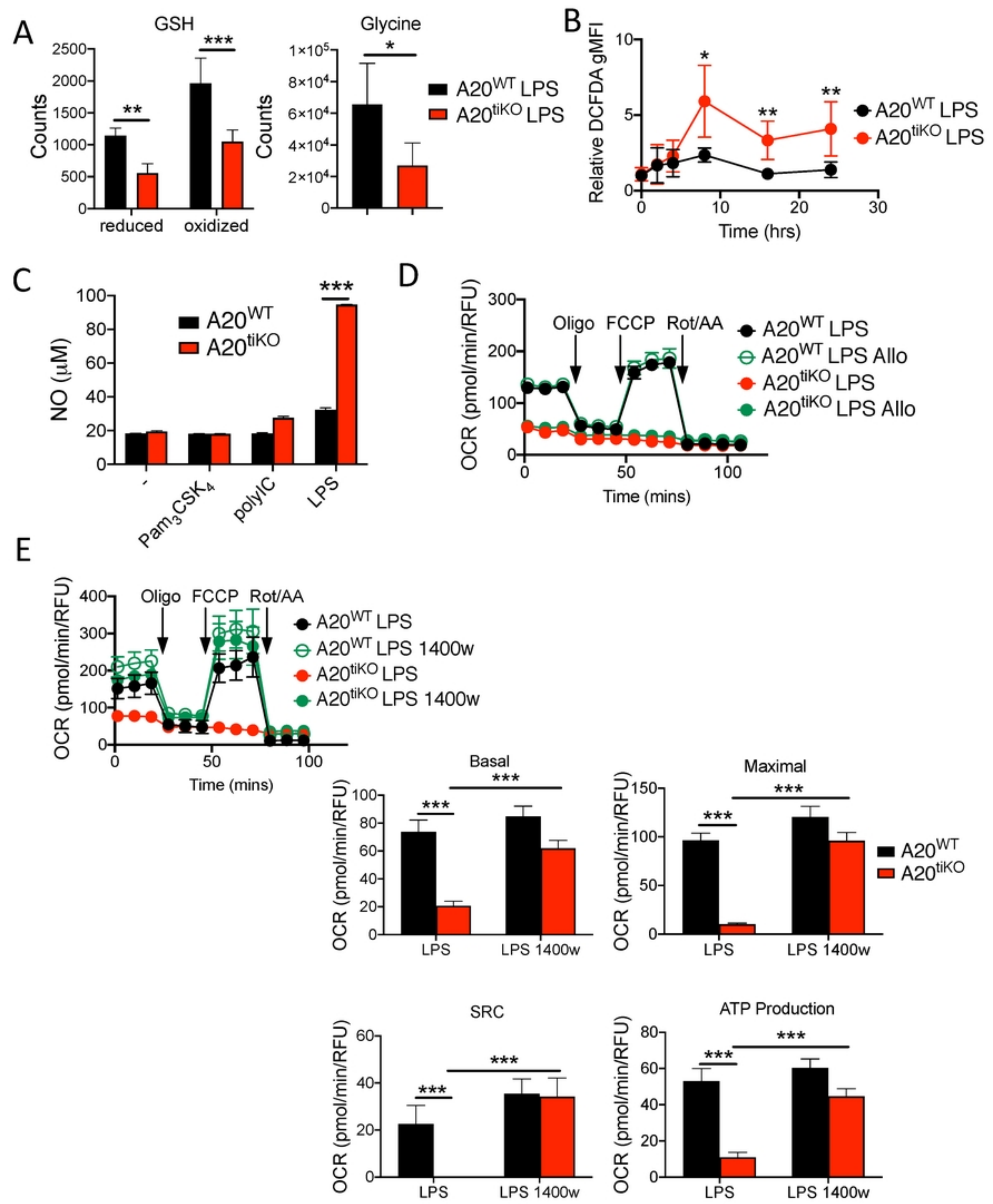

Figure 4

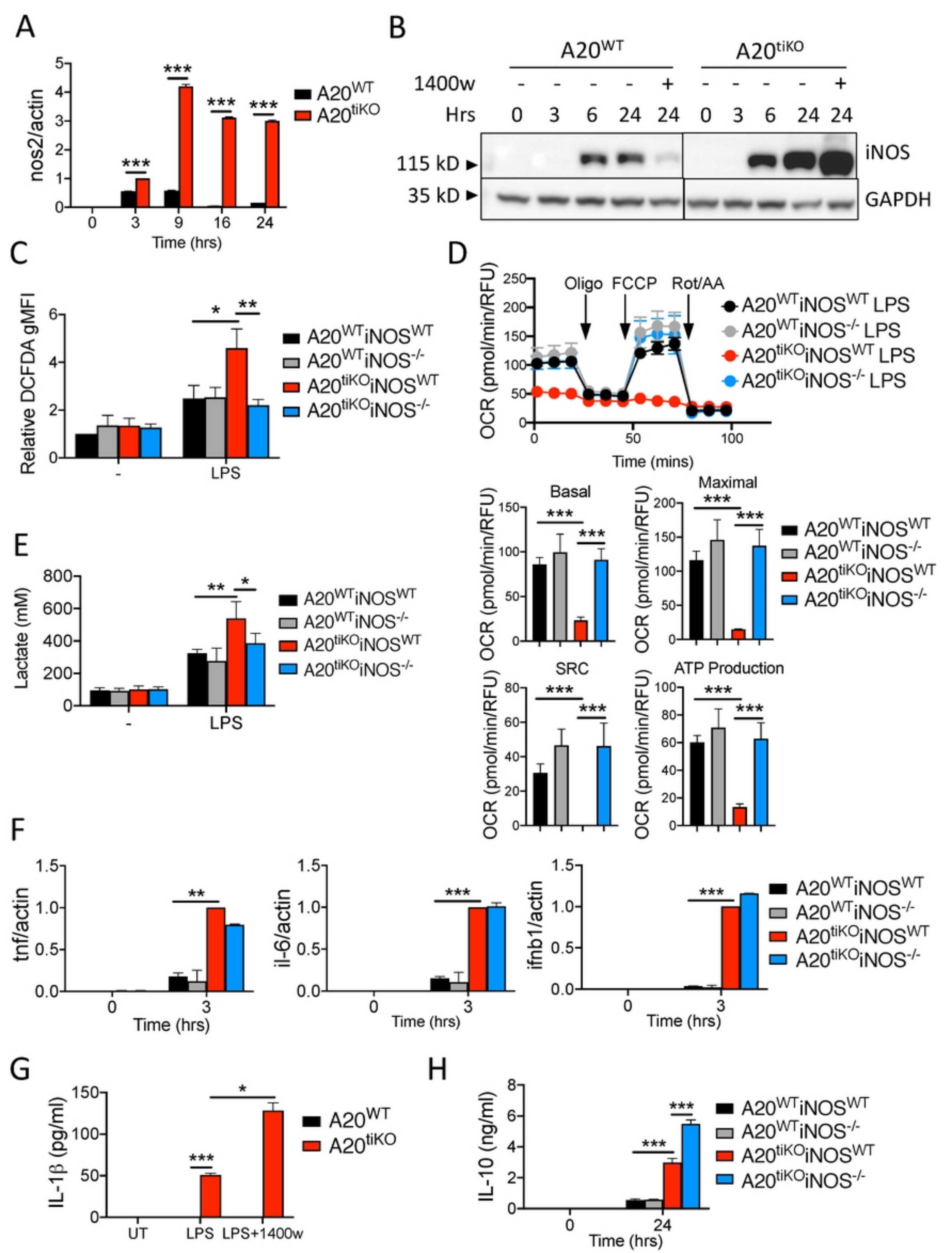
A
nos2/actin
Time (hrs)
A20WT
A20tiKO
B
A20WT
A20tiKO
1400w
Hrs
115 kD
35 kD
iNOS
GAPDH
C
Relative DCFDA gMFI
A20WTiNOSWT
A20WTiNOS-/-
A20tiKOiNOSWT
A20tiKOiNOS-/-
LPS
D
OCR (pmol/min/RFU)
Oligo
FCCP
Rot/AA
Time (mins)
A20WTiNOSWT LPS
A20WTiNOS-/- LPS
A20tiKOiNOSWT LPS
A20tiKOiNOS-/- LPS
Basal
Maximal
SRC
ATP Production
E
Lactate (mM)
F
tnf/actin
il-6/actin
ifnb1/actin
Time (hrs)
G
IL-1β (pg/ml)
UT
LPS
LPS+1400w
H
IL-10 (ng/ml)

Figure 5